Linear analysis of plasma pressure-driven mode in reversed shear cylindrical tokamak plasmas

Ding-Zong Zhang(张定宗)[1,2], Xu-Ming Feng(冯旭铭)[1,2], Jun Ma(马骏)[2,†], Wen-Feng Guo(郭文峰)[2,‡], Yan-Qing Huang(黄艳清)[1], and Hong-Bo Liu(刘洪波)[1]

[1] *College of Physics and Electronic Engineering, Hengyang Normal University, Hengyang* 421008, *China*
[2] *Institute of Plasma Physics, Chinese Academy of Sciences, Hefei* 230031, *China*

(Received 18 February 2022; revised manuscript received 25 April 2022; accepted manuscript online 18 May 2022)

The linear behavior of the dominant unstable mode ($m = 2$, $n = 1$) and its high order harmonics ($m = 2n$, $n \geq 2$) are numerically investigated in a reversed magnetic shear cylindrical plasma with two $q = 2$ rational surfaces on the basis of the non-reduced magnetohydrodynamics (MHD) equations. The results show that with low beta (beta is defined as the ratio of plasma pressure to magnetic field pressure), the dominant mode is a classical double tearing mode (DTM). However, when the beta is sufficiently large, the mode is driven mainly by plasma pressure. In such a case, both the linear growth rate and mode structures are strongly affected by pressure, while almost independent of the resistivity. This means that the dominant mode undergoes a transition from DTM to pressure-driven mode with the increase of pressure, which is consistent with the experimental result in ASDEX Upgrade. The simulations also show that the distance between two rational surfaces has an important influence on the pressure needed in mode transition. The larger the distance between two rational surfaces, the larger the pressure for driving the mode transition is. Motivated by the phenomena that the high-m modes may dominate over low-m modes at small inter-resonance distance, the high-m modes with different pressures and q profiles are studied too.

Keywords: magnetohydrodynamics (MHD), double tearing mode, pressure-driven mode

PACS: 52.55.Tn, 52.65.–y, 52.35.Py, 52.30.Cv **DOI:** 10.1088/1674-1056/ac70b4

1. Introduction

Recently, renewed attention has been paid to the reversed magnetic shear profile for its capacity of obtaining higher bootstrap current fraction, forming internal transport barrier, and improving energy confinement.[1,2] Therefore, the reversed magnetic shear configuration is considered as an advanced operation scenario to reach tokamak steady-state operation. However, for such a magnetic configuration, it often encounters some problems, such as the degradation of energy confinement, decrease of the electron temperature, and even disruptions of plasma discharge.[3,4] It is believed that these behaviors are closely correlated with the resistive double tearing mode (DTM) for the existence of two rational surfaces in this configuration. In the device of Axially Symmetric Divertor Experiment (ASDEX) Upgrade, the DTM results in the breakdown of transport barrier and decrease of the electron temperature.[5] In the Experimental Advanced Superconducting Tokamak (EAST) 2015–2018 campaign, all values of $\beta_N = \beta_t/(I_p/aB_t)$ decrease during DTM phase, but present different β_N behaviors thereafter (with β_N recovering or not).[6] Here, β_t is the toroidal beta, I_p is the plasma current, a is the minor radius, and B_t is the toroidal field on the axis. In the Japan Atomic Energy Agency Tokamak Upgrade (JT-60 U), $m = 3$, $n = 1$ DTM plays a crucial role in disruption.[7]

The typical characteristic of DTM is that there exist two rational surfaces with the same q value ($q = m/n$). The distance between these two rational surfaces plays a significant role in the linear growth rate γ, mode structure, and the nonlinear evolution of DTMs.[8,9] If the distance between the two rational surfaces is large enough to ignore the coupling between two tearing modes on resonant surfaces, the linear growth rate γ, mode structure, and magnetic island evolution are essentially identical to those of the ordinary single tearing mode. When the separation of two rational surfaces is small, two tearing modes on rational surfaces are coupled together, leading to an increase in the linear growth rates of DTM. Its resistive scaling law can be estimated from $\gamma \propto \eta^{1/3}$ rather than the resistive scaling law of the single tearing mode $\gamma \propto \eta^{3/5}$.[10] Here, η is the resistivity. In the nonlinear evolution process, the nonlinear behavior of DTM is also strongly associated with the separation between two rational surfaces. Under a certain inter-resonance distance, the inner magnetic islands and the outer islands expand toward the X points of each other, resulting in the formation of Sweet–Parker (SP) current sheets and the occurrence of flow-driven magnetic reconnection.[11,12] This explosive magnetic reconnection behavior may induce more complex nonlinear behavior, such as the formation and evolution of secondary islands and tertiary islands.[13–15] For sufficiently closed rational surfaces,

†Corresponding author. E-mail: junma@ipp.ac.cn
‡Corresponding author. E-mail: wfguo@ipp.ac.cn

© 2023 Chinese Physical Society and IOP Publishing Ltd

high-m modes may dominate over low-m modes and the DTM has broad linear spectra.[16,17] Other effects on DTM, such as toroidal or poloidal shear flows,[18] Hall effect,[19] guiding field,[20] viscosity,[21] anomalous electron viscosity effect,[22] and self-induced Alfven resonance,[23] have also been investigated.

Most of the numerical studies of DTM are based on the RMHD model, which is deduced from the full MHD model in the approximation of high-aspect-ratio and low beta. However, the plasma pressure is often relatively large in actual tokamak plasma discharge, the low pressure approximation may not be preferable, especially in future high-beta fusion reactors, such as CFETR and ITER. It is found that a finite beta can lead to multiple branch instabilities of the DTM in small rational separation, and the effects of pressure on DTM are investigated.[24] In the present work, based on the full MHD model,[13–15] the unstable modes in the presence of two $q = 2$ rational surfaces are considered. It is found that the dominant mode undergoes a transition from conventional DTM to pressure-driven mode with the increase of pressure, which is consistent with the experimental results in ASDEX Upgrade.[5] Both the linear analysis of this pressure-driven mode ($m = 2$, $n = 1$) and its high order harmonics ($m = 2n$, $n \geq 2$) are studied.

2. Simulation model

2.1. Full MHD model

The instability considered in this paper is generated in the cylindrical tokamak with the plasma minor radius a and major radius R_0. The non-reduced compressible MHD equations can be given as follows:

$$\partial_t \rho + \nabla \cdot (\rho \boldsymbol{V}) = 0, \tag{1}$$

$$\rho \partial_t \boldsymbol{V} + \rho \boldsymbol{V} \cdot \nabla \cdot \boldsymbol{V} = -\nabla P + \boldsymbol{J} \times \boldsymbol{B} + \nu \nabla^2 \boldsymbol{V}, \tag{2}$$

$$\partial_t P = -\boldsymbol{V} \cdot \nabla P - \Gamma P \nabla \cdot \boldsymbol{V} + (\Gamma - 1)\eta |\boldsymbol{J}|^2, \tag{3}$$

$$\partial_t \boldsymbol{B} = -\boldsymbol{\nabla} \times \boldsymbol{E}, \tag{4}$$

$$\boldsymbol{E} + \boldsymbol{V} \times B = \eta \boldsymbol{J}, \tag{5}$$

$$\boldsymbol{J} = \nabla \times \boldsymbol{B}, \tag{6}$$

$$\nabla \cdot B = 0, \tag{7}$$

where ρ, $\boldsymbol{V}$, P, $\boldsymbol{J}$, $\boldsymbol{B}$, ν, Γ, η, and $\boldsymbol{E}$ are the plasma density, velocity, pressure, current density, magnetic field, viscosity, adiabatic coefficient, resistivity, and electric field, respectively.

In the calculation, $\nu = 1 \times 10^{-10}$, $\Gamma = 5/3$ and the following normalizations are used: $\rho/\rho_{00} \to \rho$, $P/(B_{00}^2/\mu_0) \to P$, $\boldsymbol{V}/V_{\rm A} \to \boldsymbol{V}$, $\boldsymbol{B}/B_{00} \to \boldsymbol{B}$, $\boldsymbol{J}/(B_{00}/\mu_0) = \boldsymbol{J}$, $\nu/(V_{\rm A}\rho_{00}) \to \nu$, $\eta/(\mu_0^2 a/\tau_{\rm A}) \to \eta$, $r/a \to r$, $R_0/a \to R_0$, $t/\tau_{\rm A} \to t$, in which ρ_{00} and B_{00} are constants. $V_{\rm A} = \sqrt{B_{00}^2/\rho_{00}\mu_0}$ is the Alfven speed, and $\tau_{\rm A} = a/V_{\rm A}$ is the Alfven time.

Within the scope of linear problem, each variable can be split into an equilibrium part and a perturbation part. For example, $\rho = \rho_0 + \tilde{\rho}$, where ρ_0 and $\tilde{\rho}$ denote the equilibrium and the perturbation part of plasma density, respectively. Substituting this form of variable into the above equations, we can obtain

$$\partial_t \tilde{X} = A\tilde{X}, \tag{8}$$

where $\tilde{X}(r,\theta,\varphi,t) = (\tilde{\rho}, \tilde{V}_r, \tilde{V}_\theta, \tilde{V}_\varphi, \tilde{P}, \tilde{B}_r, \tilde{B}_\theta)^{\rm t}$, and A is a 7×7 matrix, whose elements are a function of equilibrium variables and spatial operators such as ∂_r, ∂_θ, and ∂_φ.

2.2. Numerical approach

Considering the periodicity in θ direction and φ direction, the perturbation $\tilde{X}$ can be expanded by Fourier series, *e.g.*,

$$\tilde{X}(r,\theta,\varphi,t) = \sum_{m,n} \tilde{X}_{m,n}(r)\, {\rm e}^{\gamma t + {\rm i}(m\theta - n\varphi)}, \tag{9}$$

where $\tilde{X}_{m,n}(r)$ denotes the radial profile of perturbation and γ is the linear growth rate. Substituting Eq. (9) into Eq. (8) with the help of $\partial_t \to \gamma$, $\partial_\theta \to {\rm i}m$, and $\partial_\varphi \to {\rm i}n$, equation (8) can be further changed into

$$\gamma \tilde{X}_{m,n}(r) = A_{m,n}\tilde{X}_{m,n}(r), \tag{10}$$

where $A_{m,n}$ is a matrix, $\tilde{X}_{m,n}(r) = (\tilde{\rho},\ \tilde{V}_r,\ \tilde{V}_\theta,\ \tilde{V}_\varphi,\ \tilde{P},\ \tilde{B}_r,\ \tilde{B}_\theta)^{\rm t}_{m,n}$ is the eigenvector, and γ denotes the eigenvalue. In the radial direction a 4th order finite element discretization and Galerkin method on the operators ∂_r, ∂_{rr}^2 are used.[25] More details can be found in the appendix of our previous paper.[13] The numerical code used here is the same as that in our previous work.[26] In the numerical calculation, the perfect conducting wall is used as the boundary condition.

2.3. Equilibrium

The original equilibrium of safety factor is constructed as follows:

$$q(r) = q_0 \cdot m/n \cdot F_1(r) \cdot \left[1 + \left(\frac{r}{r_0}\right)^{2\mu_0}\right]^{1/\mu_0}. \tag{11}$$

where

$$F_1(r) = 1 + f_1 \exp\left[-\left(\frac{r - r_{11}}{r_{12}}\right)^2\right],$$

$f_1 = -0.238$, $r_{11} = 0.4286$, $r_{12} = 0.304$, $m = 2$, $n = 1$,

$$r_0 = r_{\rm A}\left|\left(\frac{1}{q_0}\right)^{\mu_0} - 1\right|^{-1/2\mu_0},$$

$r_{\rm A} = 0.655$, $\mu_0 = 3.8824$, and q_0 is a constant, which is used to control the distance between the two rational surfaces Δr. The initial pressure profile is set to be $P = P_0(1 - r^2)^2$, where $P_0 = \frac{1}{2}\beta_0$, and β_0 is the beta on the axis. Unless otherwise stated, $q_0 = 1.293$, and $\eta = 2 \times 10^{-7}$. The initial radial profile of the pressure and the safety factor are both shown in Fig. 1.

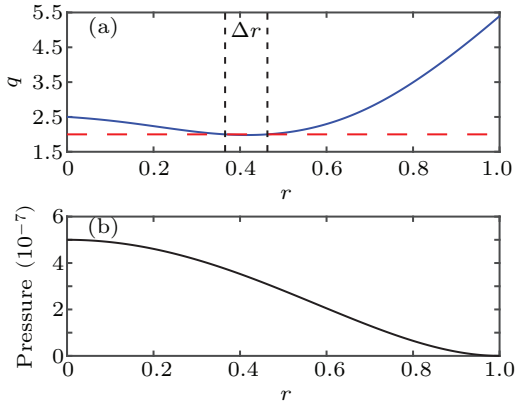


Fig. 1. Initial equilibrium radial profile of the pressure and safety factor, with Δr denoting distance between two resonant surfaces.

3. Simulation results and discussion

Firstly, the characteristics of unstable mode with an extremely low beta ($\beta_0 = 1.0 \times 10^{-6}$) are investigated. The results show that the unstable mode is essentially a DTM. Figures 2 and 3 show the eigenmode (unless otherwise stated, $m = 2$, $n = 1$) structures of radial velocity and radial magnetic field for $\Delta r = 0.1$ and 0.3, respectively. In the case of $\Delta r = 0.1$, the two resonant surfaces are well coupled with each other, and the amplitude of radial velocity is almost a constant between the two resonant surfaces (see Fig. 2(a)). This indicates that convection occurs mainly between the two resonant surfaces. The radial magnetic field is active in the region $0 < r < r_2$ and primarily in $r_1 < r < r_2$ as shown in Fig. 2(b). Here, r_1 and r_2 denote the location of the inner and outer resonant surface, respectively. For the case of $\Delta r = 0.3$, two individual modes each with a small amplitude near the two resonant surfaces can be clearly observed, and the radial velocity and radial magnetic field are greatly broadened (see Fig. 3). While other characters are very similar to those in Fig. 2. It needs pointing out that this broadening is mainly caused by the increase of separation between the two resonant surfaces. The above results resemble those in previous researches.[9,16]

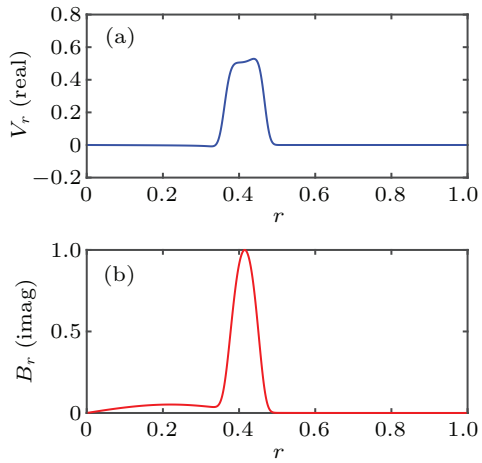


Fig. 2. Eigenmode structure of DTM for (a) radial velocity and (b) radial magnetic field with $\Delta r = 0.1$, with all variables normalized by $\max|B_r|$.

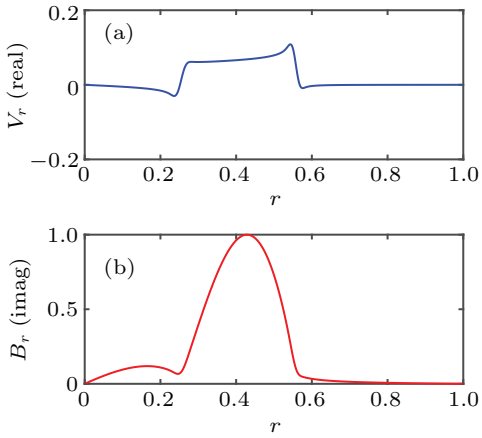


Fig. 3. Eigenmode structure of DTM for (a) radial velocity and (b) radial magnetic field, with $\Delta r = 0.3$.

Figure 4 shows the linear growth rates *versus* plasma resistivity with different values of Δr. From Fig. 4(a) we can find that the growth rate γ scales as $\eta^{1/3}$ when the Δr is 0.1. With the Δr increasing to 0.35, the scaling of DTM undergoes a transition from $\eta^{1/3}$ to $\eta^{3/5}$ as shown in Fig. 4(b). These consist well with the linear theory about DTM.[8]

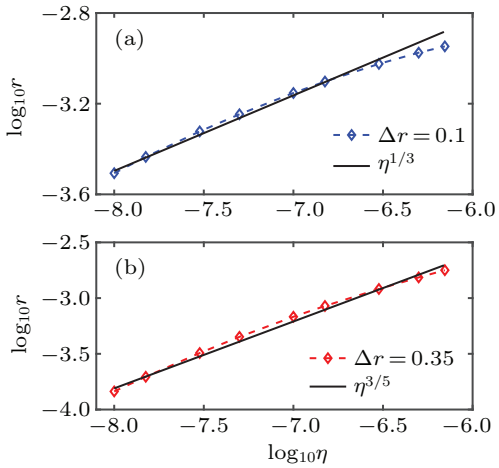


Fig. 4. Linear growth rates *versus* plasma resistivity with different values of Δr.

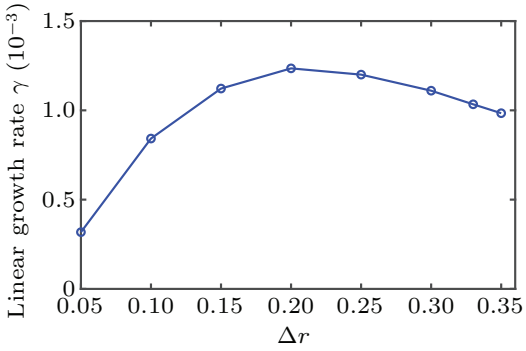


Fig. 5. Variation of linear growth rate γ with Δr.

The dependence of growth rate γ on Δr is plotted in Fig. 5 by changing q_0 in a range of 1.18–1.30, which corresponds to $0.05 \leq \Delta r \leq 0.35$. It is clear that the linear growth rate first increases and then decreases with the increase of Δr. This is

in good agreement with the results of Fig. 7 in Ref. [5] and Fig. 2 in Ref. [9].

To explore the unstable mode in high pressure regime, the eigenmode structure is plotted as indicated by blue lines in Fig. 6 with the plasma beta increasing from 1.0×10^{-6} to 0.02, while other parameters are identical to those in Fig. 2. Interestingly, the amplitude of radial velocity increases from 0.5 to 0.84, accompanied by a wide broadening in $0<r<r_2$, as shown in Fig. 6(a). This is different from the typical DTM structure, in which the radial velocity is mainly restricted between two rational surfaces $r_1<r<r_2$ (see Fig. 2(a)). In addition, an amazing change appears in the radial magnetic field (see the blue line in Fig. 6(b)). The local maximum magnetic field value in $0<r<r_1$ becomes negative, and its magnitude is almost doubled in $r_1<r<r_2$. This is also different from the radial magnetic field distribution of typical DTM. In DTM the signs of local maximum magnetic field in $0<r<r_1$ and $r_1<r<r_2$ are the same and the radial magnetic field is active primarily in $r_1<r<r_2$. These differences imply that it may be inappropriate to regard this mode as a DTM. As is well known, the DTM is essentially a resistive mode. Considering this point, an additional calculation with the resistivity set to be 0 is conducted (see the red line in Fig. 6). Clearly, no obvious difference can be found except the amplitude of radial velocity. This shows that the resistivity has very little effect on the mode structure, which is also different from the effect of resistivity on the classical DTM. To sum up, the mode structure may be a result of plasma pressure instead of resistivity. Based on this, an inference may take place in the mode in Fig. 6, which is essentially a pressure-driven mode.

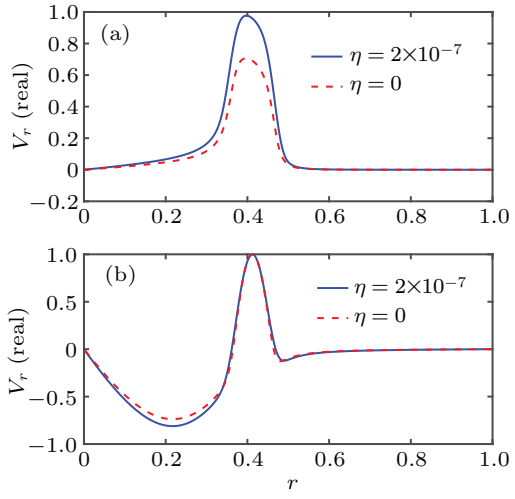


Fig. 6. Mode structures of (a) radial velocity and (b) radial magnetic field with $\beta=0.02$.

In order to confirm the above inference, the linear growth rate dependence on the plasma beta and resistivity are investigated. Figure 7 shows the effects of plasma beta on the linear growth rate, other parameters are the same as those in Fig. 2. It is obvious that the linear growth rate increases monotonically with the augment of plasma beta. Figure 8 shows the effects of resistivity on the linear growth rate in the case of four different plasma beta values, in which the same results can be obtained, namely the linear growth rate is almost independent of the resistivity. Furthermore, in the non-resonant situation ($q_{\min}=2.001$), the unstable mode can still be driven by plasma pressure.

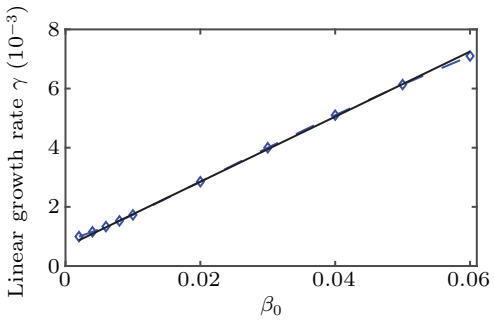


Fig. 7. Linear growth rate γ *versus* β_0.

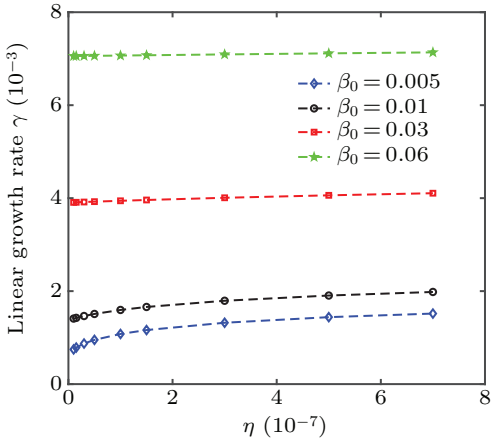


Fig. 8. Plots of linear growth rates γ *versus* η for different values of β_0.

Summarizing the results of Figs. 2–8, we can conclude that a dominant mode transition from DTM to plasma pressure-driven mode occurs with the increase of plasma beta. This transition can perhaps explain the experimental results in ASDEX Upgrade.[5] It is found that in the discharge #12224 with pure NBI hearting (*i.e.*, low beta regime) the unstable mode is DTM according to both experimental and numerical stability analysis. While in the discharge #12229 with combined NBI and ECRH (*i.e.*, high beta regime), the unstable mode becomes an ideal mode driven by the pressure. In addition, the transition from ideal to resistive mode is observed during the decrease of the electron temperature (*i.e.*, the decrease of the beta) as shown in Figs. 10 and 12 in Ref. [5], which is consistent with the numerical analysis presented in this work. In this pressure-driven mode (PDM), both the mode structure and growth rate are strongly affected by plasma pressure, while resistivity has very little effect. For simplicity, once the signs of local maximum magnetic field in $0<r<r_1$

and $r_1 < r < r_2$ become opposite and the growth rate becomes a stronger relationship with plasma pressure than resistivity, the corresponding mode is regarded as being dominated by PDM. Figure 9 shows the plot of plasma beta needed for mode transition *versus* Δr. It is found that the smaller the Δr, the more easily the transition to PDM can be triggered.

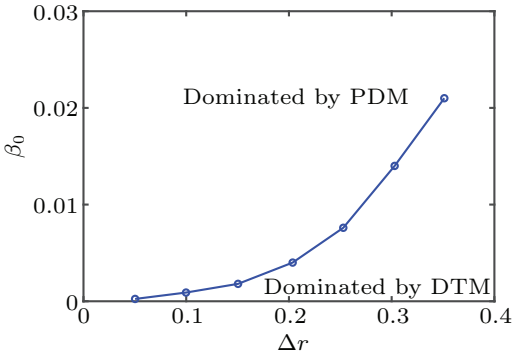


Fig. 9. Plot of β_0 needed for mode transition *versus* Δr.

In previous researches,[16,17] it is found that in small Δr the high-m modes may dominate over low-m modes and the DTM has broad linear spectra. However, in these contributions, the effects of the plasma beta are not included due to the limitation of the reduced MHD model. Then, a straight question arises: "what is the case when the plasma beta is considered?" Motivated by this question, the linear growth rates of modes with different poloidal mode numbers are investigated for different inter-resonance distances and different plasma betas.

The simulation results show that although the nature of mode has changed fundamentally with consideration of the pressure, the high-m modes ($m = 2n$, $n \geq 2$) still dominate over low-m modes in small values of Δr (see Fig. 10, in which the growth rates *versus* the poloidal mode number for different plasma betas, with Δr fixed at 0.05, 0.1, and 0.2 are plotted). In addition, the growth rate of mode first increases and then reduces with the augment of poloidal mode number in the case of small Δr, and the mode number of the fastest growing mode shifts to higher m mode with Δr decreasing (see Figs. 10(a) and 10(b)), these consist well with the results of Ref. [16]. Furthermore, in the case of small Δr, increasing beta can also result in fastest growing mode shifting to higher-m mode. For example, in the case of $\Delta r = 0.05$ (see Fig. 10(a)) the fastest-growing mode is the $m = 10$ mode when beta is 1.0×10^{-6}. When beta increases to 4.0×10^{-3}, the fastest-growing mode turns into $m = 12$ mode. Further increasing beta to 2.0×10^{-2}, the fastest-growing mode shifts to $m = 16$ mode. However, no dominant higher-m modes are destabilized with the increase of beta in large Δr (see Fig. 10(c)).

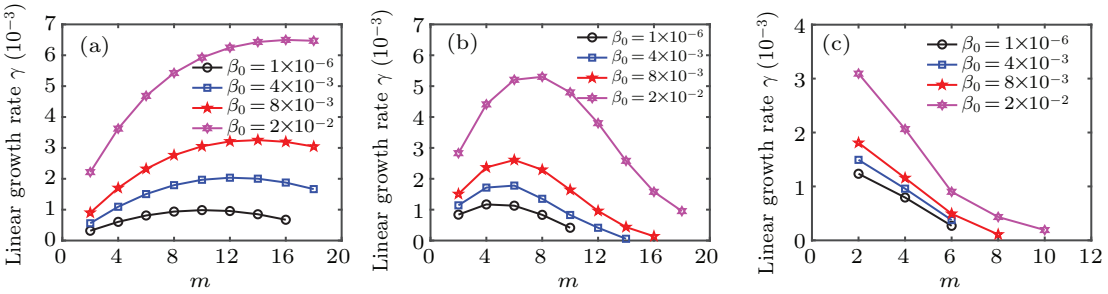


Fig. 10. Variations of linear growth rate with poloidal mode number m for different values of plasma beta with (a) $\Delta r = 0.05$, (b) $\Delta r = 0.1$, (c) $\Delta r = 0.2$.

4. Conclusions

Based on the full MHD model, the transition from DTM to pressure-driven mode is studied in reversed magnetic shear plasma. The results show that the plasma pressure has a significant influence on mode structure and growth rate. When the plasma pressure is small, the classical mode structure and growth rate scaling law of DTM can be obtained. However, the mode structure and growth rate undergo essential change when the plasma pressure is sufficiently large. Firstly, both the perturbed radial velocity and radial magnetic field are active in $0 < r < r_2$, and the magnetic field values are reverse in $0 < r < r_1$ in mode structure. Secondly, the growth rate increases monotonically with the plasma pressure and is almost independent of the resistivity. Thus this mode can be regarded as a pressure-driven mode (PDM) instead of a DTM. The results presented in the work are consistent with the experimental observations in ASDEX Upgrade. The additional computation shows that the smaller the Δr (the distance between two rational surfaces), the more easily the transition to pressure-driven mode can be triggered off. Although the nature of mode changes fundamentally with consideration of the pressure, the high-m modes still dominate over low-m modes in the case of small Δr. Like the effect of Δr on the growth rate in DTM, the growth rate of mode first increases and then decreases with y the augment of poloidal mode number in the case of small Δr, and the mode number of the fastest growing mode shifts to higher m mode with Δr decreasing. In the case of small Δr, increasing beta can also result in the fastest growing mode shifting to higher-m mode. While in the case of large Δr, no dominant higher-m modes are destabilized with the increase of pressure.

In this work, we only consider the linear physics of

pressure-driven mode in a cylinder plasma. However, the nonlinear behavior is also very important, which is one of the priorities of our next work. Generally, the flow induced by pressure-driven mode is stronger than that by DTM, and might cause stronger nonlinear evolution. The pressure driven in a cylindrical geometry plasma may be weaker than that in toroidal geometry plasma due to the toroidal effect. But the overall trend is consistent. In the future tokamak with high parameter operation, the linear and nonlinear behaviors caused by pressure will be more important.

Acknowledgements

Project supported by the Research Foundation of Education Bureau of Hunan Province, China (Grant No. 21B0648), the National Natural Science Foundation of China (Grant Nos. 11805239, 12075282, and 11775268), and the Natural Science Foundation of Hunan Province, China (Grant No. 2019JJ50011).

References

[1] Eriksson L G, Fourment C, Fuchs V, *et al.* 2002 *Phys. Rev. Lett.* **88** 145001
[2] Joffrin E, Challis C D, Conway G D, *et al.* 2003 *Nucl. Fusion* **43** 1167
[3] Snipes J A, Campbell D J, Hender T C, *et al.* 1990 *Nucl. Fusion* **30** 205
[4] ITER physics Expert Group on disruptions, Plasma Control and MHD, *et al.* 1999 *Nucl. Fusion* **39** 2577
[5] Günter S, Schade S, Maraschek M, *et al.* 2000 *Nucl. Fusion* **40** 1541
[6] Wu M F, Liu Z X, Zhang T, *et al.* 2020 *Plasma Sci. Technol.* **22** 025102
[7] Ishii Y, Masafumi A and Kishimoto Y 2002 *Phys. Rev. Lett.* **89** 205002
[8] Pritchett P L, Lee Y C and Drake J F 1980 *Phys. Fluids* **23** 1368
[9] Ishii Y, Azumi M and Tuda T 2000 *Phys. Plasmas* **7** 4477
[10] Furth H P and Killen J 1963 *Phys. Fluids* **6** 459
[11] Ishii Y, Azumi M, Kishimoto Y, *et al.* 2003 *Nucl. Fusion* **43** 539
[12] Ishii Y, Azumi M and Kishimoto Y 2003 *Phys. Plasmas* **10** 3512
[13] Guo W, Ma J and Yu Q 2019 *Plasma Phys. Control. Fusion* **61** 075011
[14] Ma J, Guo W, Yu Z, *et al.* 2017 *Nucl. Fusion* **57** 126004
[15] Guo W, Ma J and Yu Z 2017 *Phys. Plasmas* **24** 032115
[16] Bierwage A, Benkadda Sadruddin, Hamaguchi S, *et al.* 2005 *Phys. Plasmas* **12** 082504
[17] Bierwage A, Benkadda Sadruddin, Hamaguchi S, *et al.* 2007 *Phys. Plasmas* **14** 022107
[18] Zhang W, Ma Z W, Lu X Q, *et al.* 2020 *Nucl. Fusion* **60** 126022
[19] Zhang W, Ma Z W and Wang S 2017 *Phys. Plasmas* **24** 102510
[20] Pritchett P L 2005 *Phys. Plasmas* **12** 062301
[21] Zheng S, Zhang J P, Duan P, *et al.* 2013 *Acta Phys. Sin.* **62** 025205 (in Chinese)
[22] Dong J Q 1984 *Acta Phys. Sin.* **33** 1341 (in Chinese)
[23] Wei L and Wang Z X 2011 *Nucl. Fusion* **51** 123005
[24] Liu T, Yang J F, Zhao G Z, *et al.* 2017 *Plasma Phys. Control. Fusion* **59** 065009
[25] Jardin S 2010 *Computational Methods in Plasma Physics* (Boca Raton: CRC Press) pp. 301–323
[26] Guo W and Ma J 2020 *AIP Adv.* **10** 075213